Quantitative Assessment of Gas Cell Development During the Proofing of Dough by Magnetic Resonance Imaging and Image Analysis

John P. M. van Duynhoven,[1,2] Geert M. P. van Kempen,[1] Robert van Sluis,[3] Bernd Rieger,[4] Peter Weegels,[1] Lucas J. van Vliet,[4] and Klaas Nicolay[3]

ABSTRACT

The structure of bread crumb is an important factor in consumer acceptance of bakery products. The noninvasive monitoring of the gas cell formation during the proofing of dough can aid in understanding the mechanisms governing the crumb appearance in the baked product. The development of gas cells during the proofing of dough was monitored in a noninvasive manner using magnetic resonance imaging (MRI) at 4.7-T. The acquired MRI time series were analyzed quantitatively using image analysis (IA) techniques. The effects of both kneading temperature and mechanical damage by molding were studied. When additional rheological stress was introduced during molding, a more heterogeneous (coarse) gas cell size distribution was observed, and the dough had a smaller specific volume (as measured by MRI). These characteristics were preserved in the bread crumb structure after baking. The fast-deformation during molding also resulted in an isotropic growth of the dough during proofing, whereas slow-deformation during molding resulted in anisotropic growth. This can be related to a better conservation of stress in the dough under a moderate molding operation. A higher temperature during kneading also resulted in a coarser distribution of the gas cells and a smaller MRI specific dough volume. No effect of kneading temperature on the growth anisotropy could be detected, however. This indicates that temperature has a smaller effect on the conservation of stress in the dough than molding. The current work illustrates the capability of MRI/IA for understanding and predicting the influence of food processing parameters on consumer-relevant features in a food product (bread).

Cereal Chem. 80(4):390–395

The crumb structure of bread is an important factor determining the perception of bakery products by the consumer. In general, a fine crumb structure is appreciated, but in some products like *ciabatta*, flat breads, and French baguettes a coarse structure is preferred. There is an interest in the controlled manipulation of the bread crumb structure, but this requires insight into how this aspect of the microstructure evolves during the breadmaking process. One line of research focused on the relationship between bread crumb structure and the gas cell structure in the dough. Several approaches have been presented for the assessment of the gas cell structure in dough. Most directly available for the food researcher are methods that assess the gas content or density of the dough (Campbell and Mougeot 1999; Campbell et al 2001), but these do not provide a visualization of the gas cell structure. Optical and electron microscopy (Campbell 1991; Campbell et al 1991; Whitworth and Alava 1999) have been used for visualization, but these techniques are invasive and less suitable for monitoring dynamic processes in dough during proofing. Both disadvantages are overcome by using X-ray tomography, which allows the noninvasive and dynamic monitoring of gas cells during proofing (Whitworth and Alava 1999). Because this technique cannot observe gas cells with small diameters (<1 mm), we explored the use of magnetic resonance imaging (MRI).

In the last decade, we witnessed the breakthrough of magnetic resonance imaging (MRI) as a major diagnostic tool in clinical medicine (Boesch 1999). Its success can be attributed to its noninvasive nature and its ability to provide image contrast on the basis of the molecular mobility and other physicochemical properties of water (and various solutes). These capabilities have also drawn the attention of food scientists who are interested in the characterization of complex food structures. Already, at an early stage, several MRI studies were reported in the field of cereal science (Ruan et al 1996, 1999; Ruan and Chen 1998). The images produced by MRI were used to map water distribution phenomena during storage of bread (Ruan and Chen 2001; Esselink et al 2003a) and processing of cereal-based products (Gonzalez et al 2000; Kojima et al 2000). For an objective and quantitative interpretation of the features present in MRI results from the medical field, image analysis techniques have become an indispensable tool in diagnostics (Sonka and Fitzpatrick 2000). Image analysis (IA) has been established as a tool to quantify structural features in images of food, and there are several examples from the gas cell structural area (Sapirstein 1999; Whitworth and Alava 1999). In food science applications of MRI, however, the application of IA has not been introduced yet. Here we will show a successful example of the joint deployment of MRI and IA procedures for the assessment of gas cell development and anisotropy in the growth of the dough during proofing.

MATERIALS AND METHODS

Sample Preparation and Handling

The dough recipe consisted of Baguepi flour with 2.1% salt, 3.2% yeast, 1.75% bread improver (amylase, xylanase, vitamin C, Astra Calve, Creil, France), and 54% water (added at 18°C). The dough was either prepared on a laboratory scale or with an industrial processing line. On a laboratory scale, a spiral mixer (Diosna, Osnabruck, Germany) was used for kneading to optimum development, a climate cabinet (Esko, Venlo, The Netherlands) for proofing, and a molder (Tregor-1, Merand, Noyal sur Vilaine, France) for molding and shaping the baguette. For a large range of possibilities to mold the dough to baguettes on an industrial scale, a laminating line (Fritsch, Markt Einersheim, Germany) was used with a spiral mixer (Diosna) for kneading, a relaxed dough processor (RDP, Fritsch) for sheeting the dough, and an adjustable plate and belt system (Rheon, Utsonomiya, Japan) for molding and shaping the baguettes. Dough molding took place between two movable belts. For fast-deformation (7 sec), the upper belt stood still and the lower belt had a speed of 23.5 m/min. For slow-deformation (26 sec), the lower belt also moved at 23.5 m/min, but the upper belt moved counterwise at a speed of 16 m/sec. The dough pieces were blast-frozen for 35 min at –32°C, packed in sealed plastic bags, and subsequently stored at –20°C in a temperature-controlled freezer, for a period of two to three days. The dough pieces were transported to the MRI facility after being put on dry ice. After arrival at the MRI facility, the frozen dough pieces were again stored at –20°C. Within two days, the dough

[1] Unilever R&D Vlaardingen, P.O. Box 114, 3130 AC Vlaardingen, The Netherlands.
[2] Corresponding author. E-mail: John-van.Duynhoven@unilever.com.
[3] Image Sciences Institute, University Utrecht, The Netherlands.
[4] Pattern Recognition Group, Delft University of Technology, The Netherlands.

Publication no. C-2003-0614-05R.

pieces were thawed at 4°C, during an overnight period. Before the actual measurement, the samples were wrapped in cellophane and equilibrated at ambient temperature for 1 hr. The equilibration procedure ensured that the dough piece was at ambient temperature when the MRI measurement started, and prevented condensation of atmospheric water directly on the sample. The dough sample was carefully positioned and fixed on a sample holder using tape.

MRI

MRI experiments were performed at the Image Sciences Institute (University Medical Center, Utrecht, The Netherlands), using a spectrometer (Inova, Varian, Palo Alto, CA) operating at a proton frequency of 200 MHz, interfaced to an Oxford 40-cm bore, 4.7-T magnet. A standard spin-echo pulse sequence (de Graaf 1998) was used to acquire slices 3.0 mm thick. Typically, for a field-of-view of 40 × 40 or 70 × 70 mm, five slices were acquired with 0.1-mm spacing using an echo time of 9 msec and a data matrix of 256 × 256 points (in IA, only one slice was used). One data set took ≈2 min to acquire. These experiments were repeated continuously for ≈600 min. The data were processed using Vnmr and ImageBrowser software (Varian). The images were converted to the tiff format and analyzed further by image analysis.

Dough IA/MRI

Dough volume and gas cell size analysis. From the images, the cross-sectional area of the dough was measured. This parameter is defined as the MRI specific volume of the dough. The specific volume determined by MRI is likely to be equivalent to the value determined by other means because we can assume that dough elongation plays a minor role. The MRI dough specific volumes were measured as a function of proofing time.

A segmentation-based IA was used to detect and measure the gas cells during proofing. The MRI slices were segmented individually, resulting in an image containing a collection of detected gas cells for each MRI slice. The size of each gas cell was determined by counting the number of pixels. This count was stored as a two-dimensional (2-D) image versus time histogram. The segmentation of each MRI slice involved two steps: a flat-field correction for nonuniform illumination and thresholding (Russ 1995). Signal intensity variations caused by imperfections in the sensitivity profile of the MRI coil resulted in an overall increase in signal intensity from top to bottom in the images. This prohibits the use of a single threshold level to distinguish between dough and gas cells (Fig. 1A). Therefore, a flat-field correction was applied to correct for this low-frequency variation in gray values. It was applied in two steps: 1) detection of the outline of the dough (mask, used to measure the MRI specific volume of the dough), and 2) estimation of the low-frequency gray-value variations. The mask was obtained by filtering the original image with a small gray-value dilation filter (maximum filter of 5 × 5 pixels) (Fig. 1B), and to threshold the output using an isodata threshold. The low-frequency gray-value variations were found by filtering the input data (Fig. 1C) with a large Gaussian smoothing filter (using a standard deviation of 50–100 pixels). The flat-field correction was performed by dividing the pixels in the original image by the pixel values of the smoothed output (Fig. 1D). Thresholding this result would also yield objects outside the dough. This problem was solved by using the obtained mask to mask out the background. After obtaining a binary image of the gas cells (Fig. 1E), a binary opening operation on the objects was used to remove small objects (noise), and to smooth the object boundaries (Fig. 1F). Finally, the boundaries of the gas cells were extracted for display purposes (Fig. 1G). The dough analysis was performed using IA software (SCIL-Image 1.4, TNO TPD) in the form of a set of macros. In this work, the measured gas cell sizes are averaged from the slice thickness. Hence, the presented gas cell distributions are apparent ones. No attempts have been made to reconstruct the true (real) gas cell distributions by mathematical means (Campbell et al 1999).

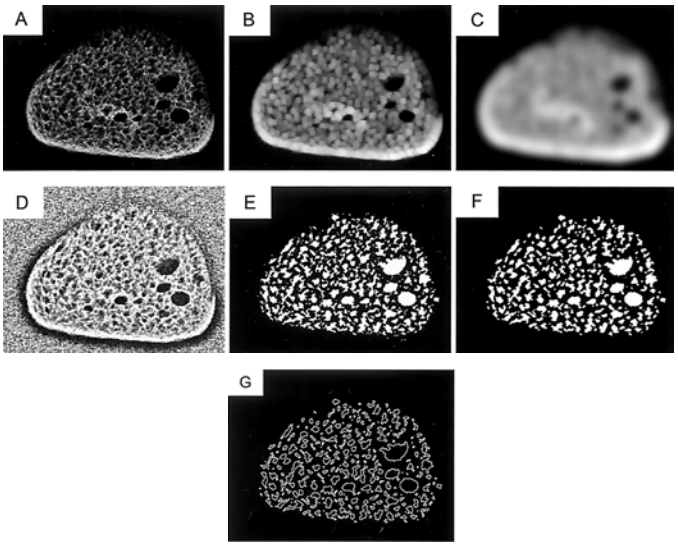

Fig. 1. Different stages in MRI analysis (all 70 × 70 mm). **A,** original MRI; **B,** after dilation filtering; **C,** after Gaussian filtering; **D,** after flat-field correction; **E,** after obtaining binary image; **F,** after binary opening operation; and **G,** after gas cell boundary definition.

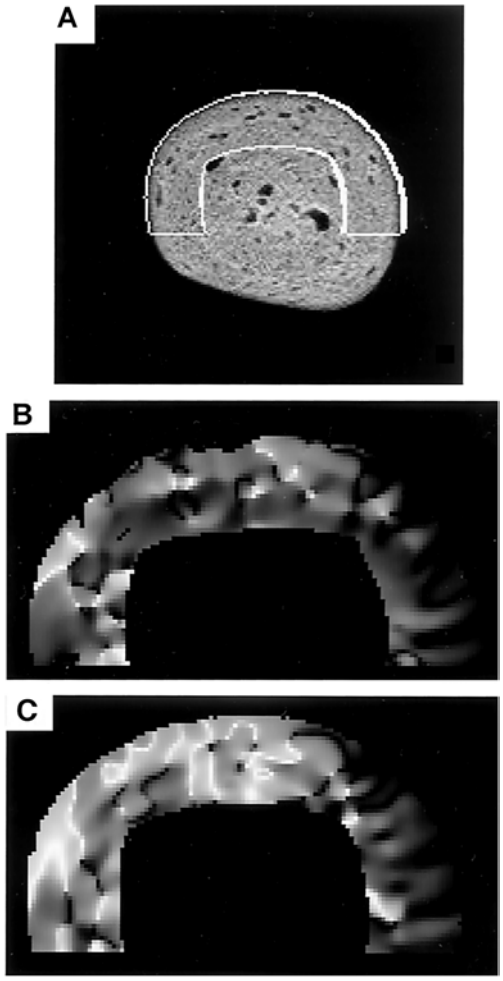

Fig. 2. Upper outer part of the dough being used for the dissimilarity measure (**A**). Angle between model and flow-field for fast-deformation (**B**) and slow-deformation (**C**). No difference is made between left or right deviation from the model. Gray level corresponds to an angle from 0 (dark) to 180 (bright) degrees.

Dough growth analysis. A gray-level IA approach was used to characterize the growth behavior during proofing. In a first step, the velocity field of the 2-D time series is obtained using optical flow (Horn and Schunck 1981). We compensated for the decreasing intensity in time in the MRI slices. The flow field was then compared with a growth model. Our growth model is an expansion model, where the growth takes place perpendicular to the contour of the dough, taking the morphology of the dough into account. By measuring relative to the crust and limiting to local analysis, we are not sensitive to rigid body rotations and transformations. Furthermore, only the upper part of the dough is evaluated because in this region the growth-restraining influence of the surface on which the dough lies is expected to be small (Fig. 2A). Hence, deviations from the modeled expansion can be directly related to the stress contained in the dough during molding. We propose a heuristic scalar dissimilarity measure. First, the angle between the velocity vector and our model direction is computed and weighted by the magnitude of the velocity vector for each position in every time slice. The weighting suppresses contributions from small vectors with large angles. Then the angles are squared and averaged inside a horse-shoe-like region (Fig. 2B and C) and normalized for the size of this area. That implies that deviations to the left and right are considered equal, and strong deviations from the model are weighed more heavily. The estimated velocity (the modulus of the displacement vector) from the optic flow acts as a confidence measure for the dissimilarity measure. The angle of the model with the flow-field is shown for this time frame in false color in Fig. 2B and C. No difference is made between left or right deviation from the model. The dough growth analysis was performed using an image processing toolbox (DIPimage for MATLAB, www.ph.tn.tudelft.nl/DIPimage, Department of Applied Physics, Delft University of Technology).

Image Conversion and Visualization

The original MRI data was stored in the MRI FDF format (32-bit floating-point data), which was read into SCIL-Image using a specially developed import filter. Once opened in SCIL-Image, the data was stretched, converted to integer values, and saved as standard 2-D gray-value tiff files. Time series of tiff files were converted to a Windows AVI file to be viewed as an animation.

RESULTS

Effect of Molding Stress

Dough was prepared on an industrial processing line, and the rheological stress imposed during molding was varied. The dough was fast- and slow-deformed in the molding step. Dough pieces were blast-frozen immediately after taking them from the line to enable transport to the MRI facility. It is known that frozen storage of dough can negatively affect the hydration state of the gluten component, and that this leads to a smaller volume after proofing and baking (Esselink et al 2003a). As a precaution, in this study the doughs were stored for short periods (two to three days), so changes in gluten hydration would be minimal. As far as such effects would occur, they would have the same impact in all of the doughs studied here. Upon arrival at the MRI facility, the dough samples were thawed. Proofing was monitored inside the

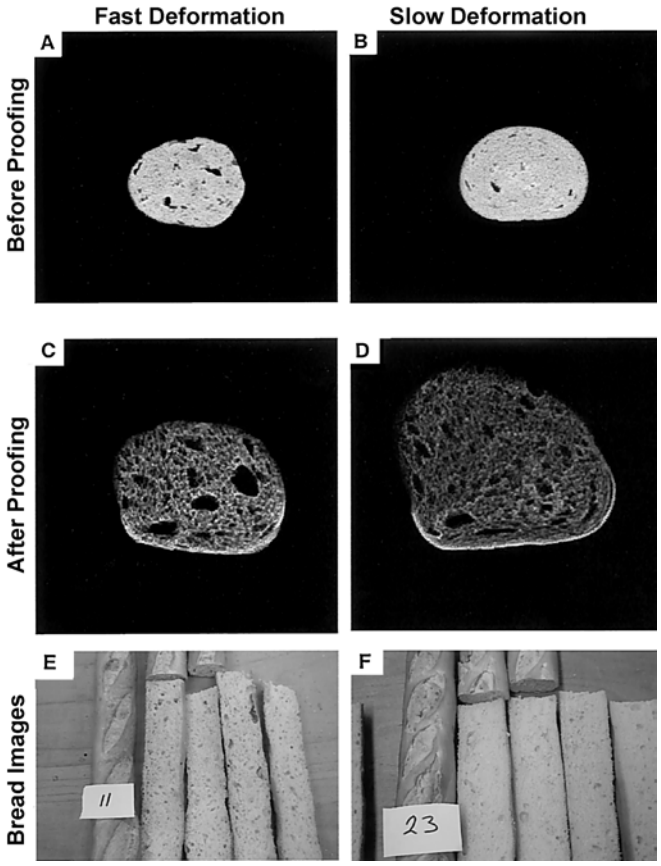

Fig. 3. Images (70 × 70 mm) of dough pieces molded with different degrees of stress: fast-deformed doughs (**A, C, E**) and slow-deformed doughs (**B, D, E**). Images taken before (**A, B**) and after (**C, D**) proofing. Bread images (**E, F**) correspond to baked dough pieces that were also fast- and slow-deformed during molding.

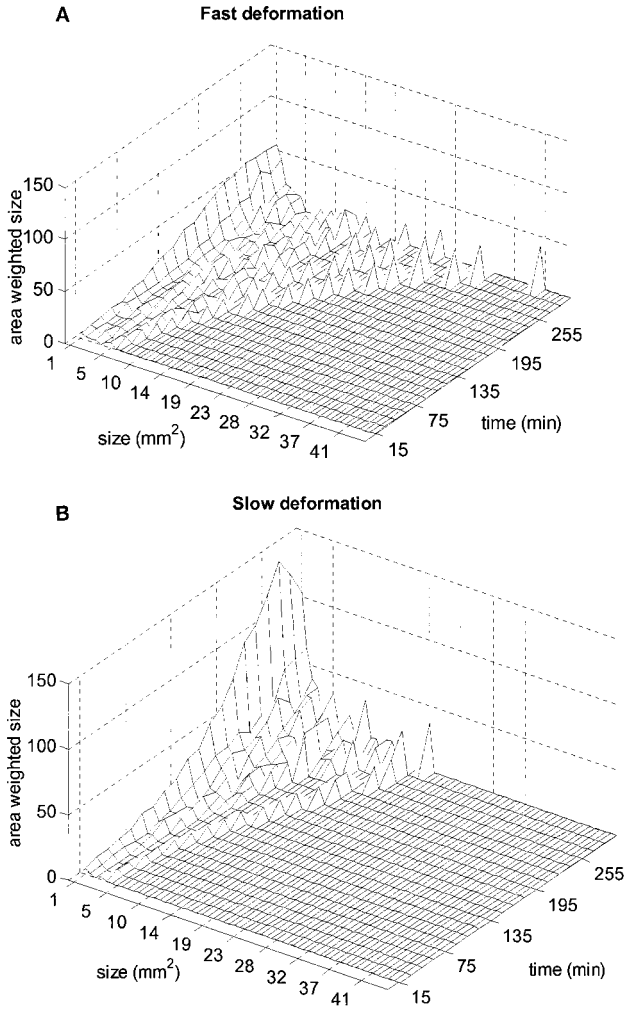

Fig. 4. Gas cell size distribution as a function of proofing time for doughs molded with different degrees of stress: fast-deformed doughs (**A**) and slow-deformed doughs (**B**).

scanner in a noninvasive manner. MRI measurements were performed in duplicate; typical images for a nonproofed dough are shown in Fig. 3 (A and B). It should be noted that with the available MRI technology, only components with sufficiently long transversal relaxation times (T_2 >10 msec) can be monitored. For dough, this means that the image reflects the presence of water molecules with sufficient mobility (Ruan et al 1999). The gas cell development was monitored continuously by repeated MRI. Images of fully proofed dough are shown in Fig. 3 (C and D). In Fig. 3, the images on the left (A, C, E) and right side (B, D, F), respectively, clearly illustrate the effect of fast- and slow-deformation on the gas cell size distribution. These effects can be observed in the dough images, as well as in the crumb structure of the baked bread (bottom images). It is clear that MRI of the fast-deformed dough has a smaller area (suggesting a lower specific volume), but also a coarser gas cell structure. IA allowed a more objective and quantitative interpretation. Typically, the procedure recognizes both smaller (0.25 mm) and larger gas cells. The gas cell size distributions were calculated for all time points taken during the dough proofing. The results for the two types of processing are shown in Figs. 4–6. The two doughs differ considerably with respect to gas cell size distribution. Fast-deformation results in a much wider (inhomogeneous) distribution (Fig. 4A). For the slow-deformed dough, a much narrower distribution is observed (Fig. 4B). The specific volume of these dough pieces can be assessed by monitoring the area in the MRI results. Slow-deformed dough pieces have a higher (MRI) specific volume during proofing (Fig. 5). The molding stress also has an impact on the degree of anisotropy of the growth of the dough. As illustrated in Fig. 6, the dissimilarity measured with the isotropic model (measure for anisotropic growth) is small for fast-deformation and larger for slow-deformation. Large dissimilarity measures (i.e., a large deviation of isotropic growth) can be attributed to the presence of internal stress in the dough. These stress lines occur in the dough during the manufacturing procedure when dough slabs are rolled into a baguette shape. Hence, if stress lines are present in the slab, they will be spiral-oriented in the resulting dough sample. If the molding step does not destroy the internal stress lines, the growth of the dough during proofing can be locally restrained by anisotropic distribution. As a result, an anisotropy in the growth will be observed. This is clearly the case for the slow-deformed samples. On the other hand, fast-deformation may cause an overstress in the dough and disrupt internal structures, in contrast to slow-deformation where they would stay intact. The loss of internal structures results in an isotropic growth of the dough. The impact of a fast-deformation on dough resembles the effect of dough extrusion (Esselink et al 2003b), where its detrimental effects on internal structures were demonstrated at the molecular and microscopic level. After baking the proofed dough, the gas cell distribution is preserved in the crumb structure of the bread (Fig. 3E,F). Hence, the crumb structure is already defined at an early stage of the breadmaking process, and baking is not the sole determining step.

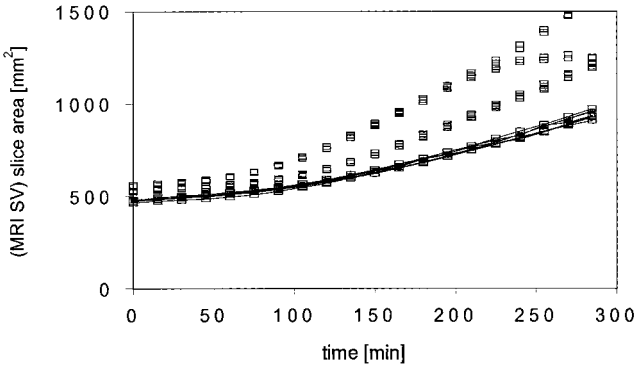

Fig. 5. Measured areas of the same dough pieces (MRI specific volume) as in Fig. 4. Slow-deformation (unconnected symbols), fast-deformation (symbols connected by lines). Model was applied on duplicate dough sample slices (5 mm apart).

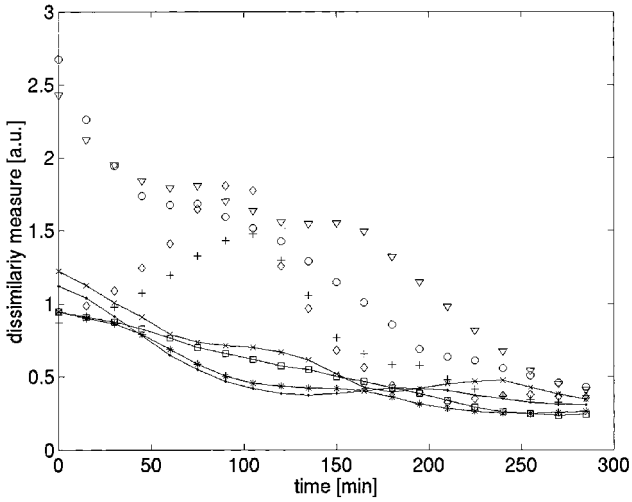

Fig. 6. Dissimilarity measure as a function of proofing time for doughs with different degrees of imposed molding stress. Slow-deformation (unconnected symbols), fast-deformation (symbols connected by lines). Model was applied on duplicate dough sample slices (5 mm apart).

Effect of Dough Kneading Temperature

The effect of dough kneading temperature was studied on a laboratory scale, where dough was kneaded at two different temperatures (26 and 28°C). From industrial manufacturing experience, these settings have an impact on the final appearance of the product. MRI measurements were performed in duplicate and typical images are shown in Fig. 7. Note that in one dough image, one can still recognize the folding of the dough slab (indicated by arrows) into the cylindrical baguette shape. These lines are parallel to the stress lines that were present in the slabs and that are preserved in the baguettes as spirals. After proofing, we observe that the dough kneaded at higher temperature has a

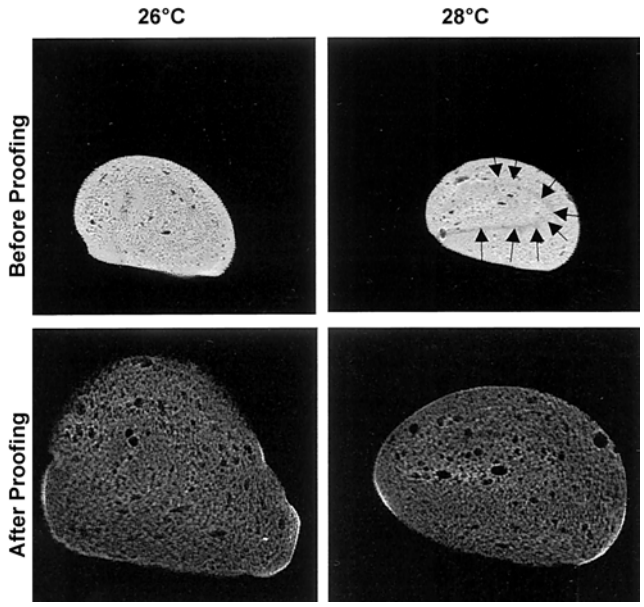

Fig. 7. MRI slices (70 × 70 mm) taken through baguette dough pieces kneaded at (left) 26°C and (right) 28°C, respectively, before (top) and after (bottom) proofing. Black arrows (top right) in the nonproofed dough image kneaded at 28°C illustrate a visible stress line introduced during molding.

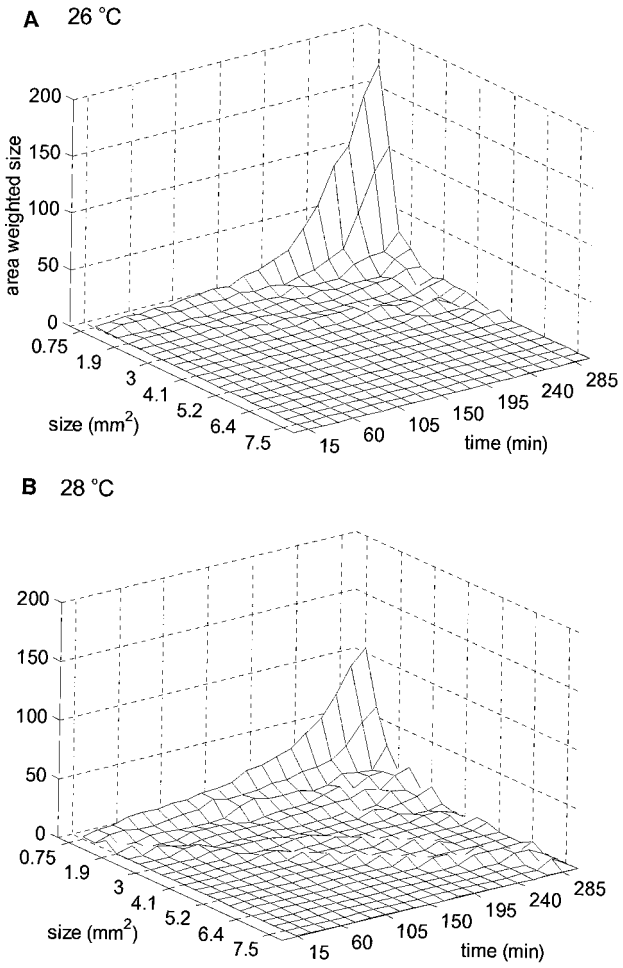

Fig. 8. Gas cell size distribution as a function of proofing time for doughs kneaded at different temperatures: **A,** 26°C and **B,** 28°C.

smaller specific volume, but also a coarser crumb structure. Using IA, the gas cell size distributions were calculated for all time points taken during the dough proofing. The results for the two dough samples are shown in Fig. 8A and B. At 26°C, the distribution of gas cells remains relatively narrow during the complete course of proofing. At 28°C, however, the gas cell distribution is wider. The impact of dough kneading temperature on dough gas cell distribution width is less clear than observed previously for variation in molding stress. The MRI-specific volumes are given as a function of proofing time in Fig. 9. The dough kneaded at 28°C has a smaller MRI-specific dough volume during proofing than the dough kneaded at 26°C. On the other hand, there was no significant effect of temperature on the growth anisotropy behavior (results not shown). Hence, we may conclude that increasing the kneading temperature can induce an effect on dough proofing behavior similar to variation of molding stress. With respect to gas cell distribution and growth anisotropy, the impact is less explicit, however.

DISCUSSION AND CONCLUSIONS

The combined use of MRI/IA allowed us to draw several conclusions on gas cell development in proofing dough and the resulting crumb structure in bread. The preset gas cell size distribution in the proofed dough is maintained further in the baking process and, consequently, largely determines the bread crumb structure. An inhomogeneous gas cell distribution can be induced by kneading the dough at higher temperature or by applying a fast-deformation during molding. In both cases, however, this effect is

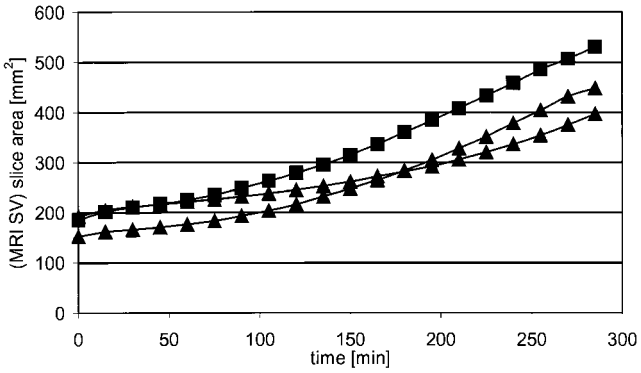

Fig. 9. Measured areas (MRI specific volumes) of dough samples kneaded at 26°C (■) and 28°C (▲).

compromised by a smaller MRI-specific dough volume. Often, a concerted motion of the cell can be observed when the gas cell development is monitored continuously. This anisotropic growth behavior follows the stress lines that are conserved in the dough after molding (sometimes these lines are visible, as in Fig. 7 for the dough kneaded at 28°C). A higher conservation of stress can be achieved by using a slow-deformation during molding. A change in kneading temperature does not have a noticeable effect on growth anisotropy, however.

In this work, we have shown the successful deployment of MRI/IA for the quantitative and noninvasive monitoring of the proofing of dough under relevant industrial conditions. To our knowledge, the quantification of MRI results, using IA techniques for the structural mapping of industrial food processing is unprecedented. The current application illustrates the potential value of the MRI/IA approach for understanding and predicting food processing parameters on consumer-relevant features in a food product (bread).

More structural detail could be derived from the MRI data if they would be recorded in 3-D mode because this would improve spatial resolution. Using time-resolved analysis of structural features, the behavior of individual gas cells could be tracked and related with predictions of modeling (Shah et al 1998).

ACKNOWLEDGMENTS

We thank M. de Man and T. Henderson for preparation and supply of dough material and useful discussions. We thank ICC Aartselaar for providing us with dough samples from industrial processing lines.

LITERATURE CITED

Boesch, C. 1999. Molecular aspects of magnetic resonance imaging and spectroscopy. Mol. Aspects Med. 20:185-318.

Campbell, G. M. 1991. The aeration of bread dough during mixing. PhD thesis. Clare College, University of Cambridge: Cambridge, UK.

Campbell, G. M., and Mougeot, E. 1999 Creation and characterisation of aerated food products. Trends Food Sci. Technol. 10:283-296.

Campbell, G. M., Rielly, C. D., Fryer, P. J., and Sadd, P. A. 1991. The measurement of bubble size distributions in an opaque food fluid. Trans. I Chem. E (Part C) 69:67-76.

Campbell, G. M., Rielly, C. D., Fryer, P. J., and Sadd, P. A. 1999. Reconstruction of bubble size distributions from slices. Pages 207-231 in: Bubbles in Food. G. M. Campbell, C. Webb, S. S. Pandiella, eds. Am. Assoc. Cereal Chem.: St. Paul, MN.

Campbell, G. M., Herrero-Sanchez, R., Payo-Rodriguez, R., and Merchan, M. L. 2001. Measurement of dynamic dough density and effect of surfactants and flour type on aeration during mixing and gas retention during proofing. Cereal Chem. 78:272-277.

de Graaf, R. A. 1998. In Vivo NMR Spectroscopy: Principles and Techniques. John Wiley and Sons: New York.

Esselink, E. F. J., van Aalst, H., Maliepaard, M., and van Duynhoven, J. P. M. 2003a. Long-term storage effect in frozen dough by spectroscopy and microscopy. Cereal Chem. 80:396-403.

Esselink, E. F. J., van Aalst, H., Maliepaard, M., van Duynhoven, J. P. M., Henderson, M. H., and Hoekstra, L. L. 2003b. Impact of industrial dough processing on structure: A rheology, nuclear magnetic resonance and electron microscopy study. Cereal Chem. 80:419-423.

Gonzalez, J. J., McCarthy, K. L., and McCarthy, M. J. 2000. Textural and structural changes in lasagna after cooking. J. Texture Stud. 31:93-108.

Horn, B. K. P., and Schunck, B. G. 1981. Determining optical flow. Artificial Intelligence 17:185-203.

Kojima, T., Sekine, M., Suzuki, T., Horigane, A., and Nagata, T. 2000. The effect of moisture distribution on texture of boiled Japanese noodles. J. Jap. Soc. Food Sci. Technol. 47:142-147.

Ruan, C., and Chen, J. 1998. Pages 149-228 in: Water in Food and Biological Materials: A Nuclear Magnetic Resonance Approach. Technomic Publishing: Lancaster, PA.

Ruan, R., and Chen, P. 2001. Pages 127-134 in: Bread Staling. CRC Press: Boca Raton, FL.

Ruan, R., Almaer, S., Huang, V. T., Perkins, P., Chen, P., and Fulcher, R. G. 1996. Relationship between firming and water mobility in starch-based food systems during storage. Cereal Chem. 73:328-332.

Ruan, R. R., Wang, X., Chen, P. L., Fulcher, R. G., Pescheck, P., and Chakrabarti, S. 1999. Studies of water in dough using nuclear magnetic resonance. Cereal Chem. 76:231-235.

Russ, J. C. 1995. The Image Processing Handbook. 2nd Ed. CRC Press: Boca Raton, FL.

Sapirstein, H. D. 1999. The imaging and measurement of bubbles in bread. Pages 233-243 in: Bubbles in Food. G. M. Campbell, C. Webb, and S. S. Pandiella, eds. Am. Assoc. Cereal Chem.: St. Paul, MN.

Shah, P., Campbell, G. M., McKee, S. L., and Rielly, C. D. 1998. Proving of bread dough: Modelling the growth of individual bubbles. Trans. I Chem. E (Part C) 76:73-79.

Sonka, M., and Fitzpatrick, J. M. 2000. Handbook of Medical Imaging. Vol. 2, Medical Image Processing and Analysis. SPIE: Bellingham, WA.

Whitworth, M. B., and Alava, J. M. 1999. The imaging and measurements of bubbles in bread doughs. Pages 221-231 in: Bubbles in Food. G. M. Campbell, C. Webb, and S. S. Pandiella, eds. Am. Assoc. Cereal Chem.: St. Paul, MN.

[Received January 11, 2002. Accepted July 22, 2002.]